Wu *et al. Earth, Planets and Space* (2023) 75:66
https://doi.org/10.1186/s40623-023-01819-2

Earth, Planets and Space

FULL PAPER

Open Access

Conjugate observations of power line harmonic radiation onboard DEMETER

Jing Wu[1*], Zhengkai Wang[1], Jingwen Zhang[1], Chao Yue[2] and Li Xie[3]

Abstract

The effects of power line harmonic radiation (PLHR) on near-Earth space have been debated for many years. Since some ultrahigh voltage AC and DC power projects were added to the Chinese power grid, increasingly numerous radiations at 50 Hz and their harmonics have been caught by the microsatellite DEMETER in the geomagnetically conjugate topside ionosphere during the daytime of winter and spring. Distribution of SYM-H index has been studied, showing geomagnetic disturbances may be unnecessary for the occurrence of PLHR. The propagation of PLHR between hemispheres without much attenuation illustrates that PLHR can be amplified when crosses the equatorial zone. Eliminating seasonal and diurnal factors, dependence of PLHR propagation on the change in plasma density is disclosed. The abrupt variation of electron density gradient may create a favored condition for PLHR waves propagating between hemispheres.

Keywords Power line harmonic radiation, Ultrahigh voltage, Satellite detection, Electron density gradient

Graphical Abstract

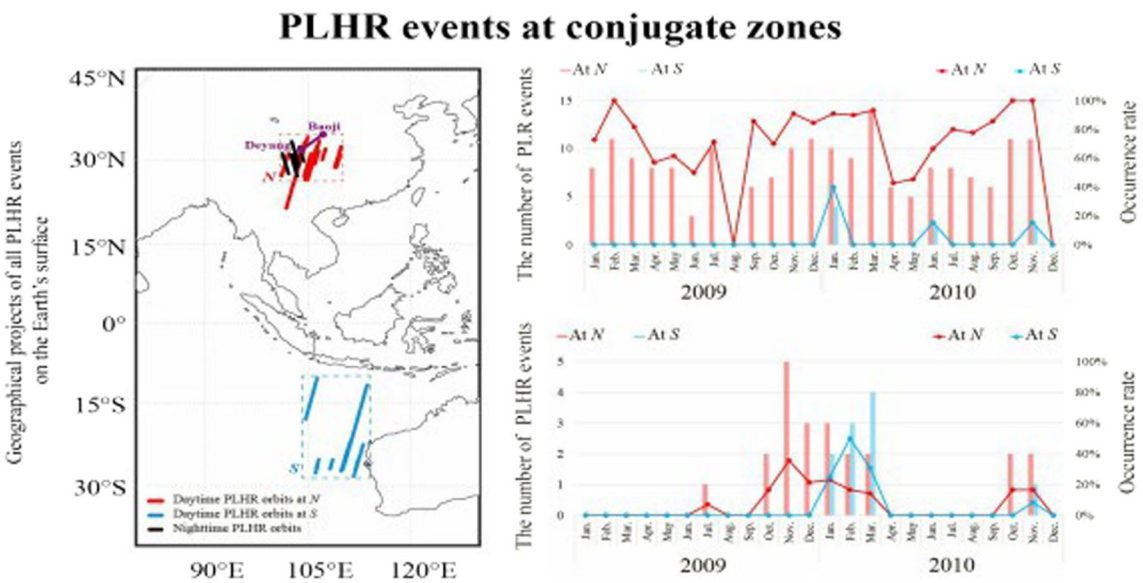

*Correspondence:
Jing Wu
wujing06@buaa.edu.cn
Full list of author information is available at the end of the article

Introduction

During the research of whistlers and their related ionospheric phenomena via observations at geomagnetically conjugate stations, a particular kind of harmonic radiation with almost constant spacings at once or twice the working frequency of the local power grid (50/60 Hz or 100/120 Hz) in the band of (1–8) kHz (Helliwell 1965), called power line harmonic radiation (PLHR), attracted wide attention. They were positively postulated to originate from the power grid in 1975 (Helliwell et al. 1975). Ground-based studies infer that PLHR can be guided by the geomagnetic field to penetrate the ionosphere and enter the inner magnetosphere and even propagate between the North and the South (Mattews and Yearby 1981; Park and Chang 1978), during which it may be greatly amplified or trigger new and stronger emissions through wave–particle interactions (Park and Helliwell 1978, 1981; Park et al. 1983). The existence of PLHR over one hemisphere side has been demonstrated by extensive satellite-based observations, including OGO-4 (Luette 1983), ISEE 1 (Bell et al. 1982), ISIS 1 and 2 (Rodger et al 1995), OHZORA (Tomizawa and Yoshino 1985), AUREOL-3 (Parrot 1994), DEMETER (Němec et al. 2007a; Parrot 2018; Wu et al. 2017), and Chibis-M (Dudkin et al. 2015). However, there have been few distinct satellite-based observations to support its propagation path and interaction with charged particles.

There is no doubt that PLHR and its triggered emissions increase the background VLF noise level in near-Earth space. This additional noise makes the experimental design for magnetospheric studies more complicated, degrades VLF communication links, and interferes with ground-based experiments (Manninen 2005). The emissions and chorus seemingly triggered and controlled by PLHR even led to a heated debate about the extent to which PLHR affects the radiation belt and the energy exchange between the magnetosphere and the ionosphere. One view is that PLHR can interact with energetic electrons in the magnetosphere and trigger strong emissions (Helliwell et al. 1975; Park and Helliwell 1978; Nunn et al. 1999; Parrot et al. 2014), and global power grids will play an important role in the dynamics and wave activity in near-Earth space (Luette 1983). The other view is that the effects of PLHR are negligible (Thorne and Tsurutani 1979, 1981; Němec et al. 2010). There were several observations supporting both of them. However, in the last 15 years, with the aid of the solar synchronous microsatellite DEMETER, an increasing number of PLHRs (Němec et al. 2007a, 2010; Parrot 2018; Wu et al. 2017, 2022) rather than their triggered emissions have been detected at low, middle, and high latitudes (Parrot 2018; Parrot and Němec 2009; Parrot et al. 2014). For example, using an automatic identification procedure, only 2 triggered events among 148 PLHR events were identified from the burst-mode data during the period of June 2004 to November 2009 (Němec et al. 2010). It is difficult to use a few triggered events to evaluate the effects of PLHR.

In this paper, we analyze the characteristics of PLHR events observed by DEMETER across zone *N* covering the geographical range of (21°N–35°N, 100°E–111°E) and its geomagnetically conjugate zone *S*: (10°S–29°S, 104°E–114°E). The northern footprints of the geomagnetic field lines across both zones are in Sichuan, China, whose power grid structure has changed greatly as the ± 500 kV Deyang-Baoji DC power project was added in the second half of 2009, and the southern footprints are above the Indian Ocean, where there has been no industrial power grid. Most importantly, the correlation between PLHR and local electron density variation is discussed, which has been rarely concerned.

Dataset and method

The microsatellite DEMETER adopted a quasi-synchronous circular orbit with an orbital inclination of approximately 98.3° at an altitude of approximately 660 km (Lagoutte et al. 2006), and its on-orbit flying time was from June 2004 to the end of 2010, during which the structure of the Chinese power grid changed considerably. In this paper, the data of electric field intensity *E* in the range of 0–20 kHz acquired by Instrument Champ Electrique (ICE) in burst mode with a sampling frequency of 40 kHz and electron density (N_e) acquired by Instrument Sonde de Langmuir (ISL) with a sampling frequency of 1 Hz are analyzed to identify PLHR events and their related plasma density changes. All the orbits mentioned hereafter are in burst mode.

Analysis of *E* data

We used the short-time Fourier transform and the Welch power spectra estimation method to analyze the *E* data (Guo et al. 2019). The frequency resolution is 1 Hz, and the feed-forward time interval is 0.8192 s for analyzing 1 s of data. In the frequency-time spectrogram, a PLHR event is defined as a cluster of parallel spectral lines (at least 3 lines) spaced by 50 Hz or 100 Hz occurring synchronously during at least 15 s along an orbit. It is worth putting out that an automatic identification procedure for the PLHR event was developed by Němec et al. (2006), and using it, many events in the range of 500–4000 Hz were identified, but there were few events over China (Parrot et al. 2014). Instead of automatic identification procedure, we manually checked the frequency–time spectrograms in 0–10 kHz. Using our procedure, all the events with a given orbit number in Němec et al. (2006, 2007a, b, 2008, 2010) have been identified, and many

events over China have also been identified (Wu et al. 2017). Here, we use it to carefully detect the power line emission (PLE) event at 50 Hz (Dudkin et al. 2015; Guo et al. 2019; Pilipenko et al. 2021) and PLHR event in the range of 4–10 kHz over central and western China and its geomagnetically conjugate zone over the Indian Ocean.

Frequency–time spectrograms of two typical PLHR events (events A and B) detected in consecutive days at zones *N* and *S* and their amplitude comparison are shown in Fig. 1a. In event A, the PLE line is almost everywhere along the orbit with a maximum intensity of 1.15 $\mu V^2 m^{-2}$ Hz^{-1}, and its frequency is the exact power grid working frequency of 50 Hz; there are 4 PLHR lines at 4153/4253/4353/4453 Hz in the magnetic latitude range MLat = 16.8°N–22°N, the magnetic *L*-shell value range *L* = 1.14–1.24, and the universal time range UT = 03:00:40–03:02:00, and their maximum frequency deviation from the exact harmonic frequencies of 50 Hz is $\Delta f = 3$ Hz. The maximum peak power spectral density (PSD) of the lines is at 4353 Hz, the value is $(PSD)_{4353\ Hz} = 0.017$ $\mu V^2 m^{-2}$ Hz^{-1}, and the total power spectral density (Total PSD) is 0.052 $\mu V^2 m^{-2}$. The ratio of the maximum PSD to the average background noise wave density is defined as the signal-to-noise ratio (SNR), and the SNR of event A is 9.42 dB. In event B, there is no PLE line, although four PLHR lines can be seen in Fig. 1a (right) at 4150/4250/4350/4450 Hz in the conjugate ranges of MLat = 22°S–33°S, *L* = 1.20–1.75 and

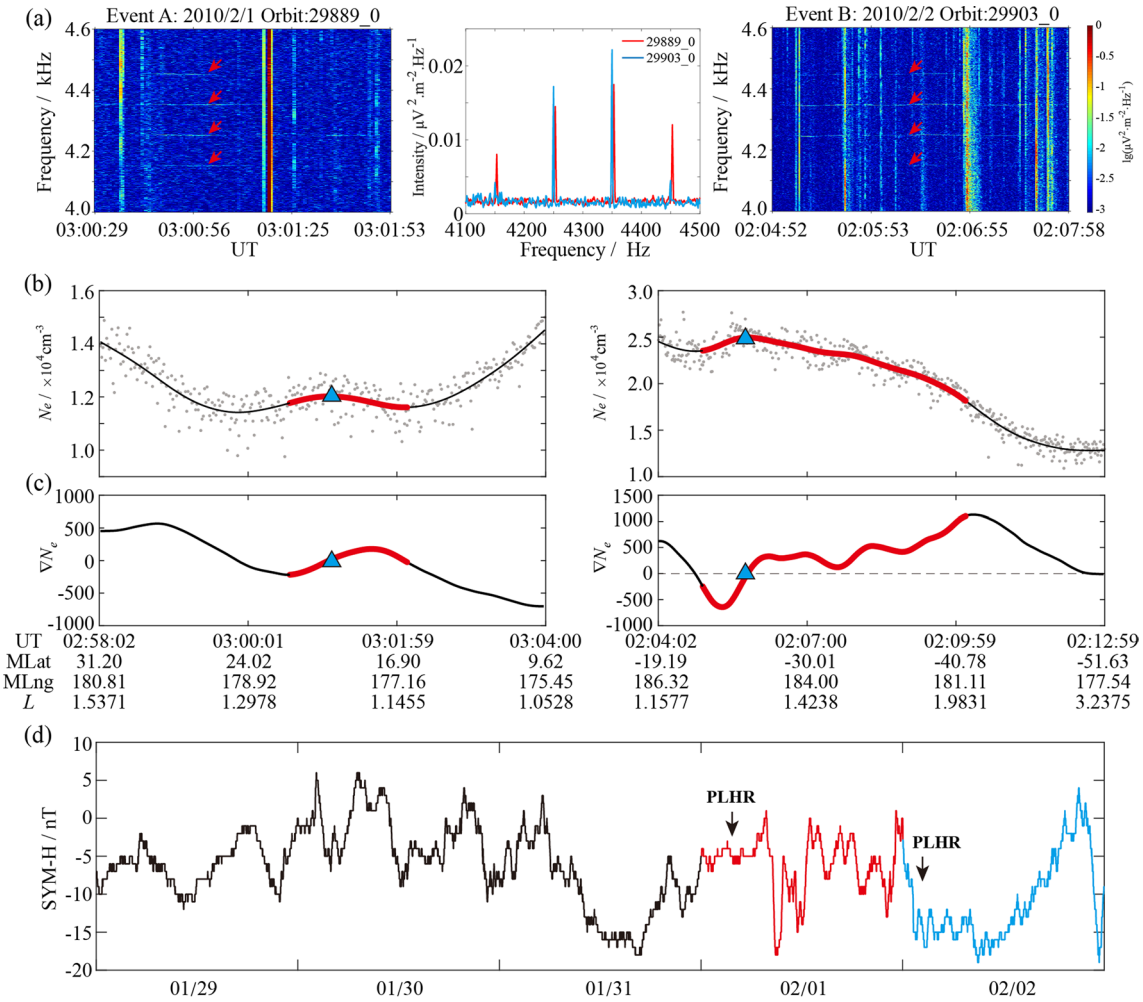

Fig. 1 Two typical PLHR events at the conjugate zones. **a** Frequency–time spectrograms of events A and B and their amplitude comparison. All PLHR lines are near 4150/4250/4350/4450 Hz and spaced by 100 Hz. The densities of the 4250 Hz and 4350 Hz lines in event B are stronger than those in event A. **b** Fluctuation of N_e. Dots are data measured by DEMETER, and they are fitted by a smoothing spline curve, where the red segment is the range of PLHR. The blue triangle represents the local peak of N_e. **c** Fluctuation of ∇N_e, where the blue triangle indicates $\nabla N_e = 0$. **d** Variation in the SYM-H index during the occurrence of PLHR and three days before PLHR. The strongest value is only − 19 nT. Line in red represents event A and line in blue represents event B

UT = 02:05:00–02:09:00, $\Delta f = 0$, $(\mathrm{PSD})_{4350\ \mathrm{Hz}} = 0.022$ $\mu V^2 m^{-2}$ Hz^{-1}, Total PSD = 0.048 $\mu V^2 m^{-2}$, and SNR = 11.38 dB. The PSD and SNR values of event B are both greater than those of event A, and the amplification ratios are 129% and 120%, respectively. The detailed information is shown in Table 1.

Analysis of N_e data

DEMETER measured N_e every second, and its range was 10^2–5×10^6 cm^{-3}. Along the orbits of events A and B, the data of N_e are shown by dots in Fig. 1b. In order to obtain the variation of electron density (N_e) depending on the latitude (MLat), spline function is used to fit the function of $N_e = g(\mathrm{MLat})$. For any point (MLat_i) along the satellite orbit, the function g satisfies:

$$\min\left\{p\sum_i\left[(N_e)_i - g(\mathrm{MLat}_i)\right]^2\right\} + (1-p)\int\left(\frac{\mathrm{d}^2 g}{\mathrm{d}x^2}\right)\mathrm{d}x, \tag{1}$$

where p is called the smoothing factor. It is found that when $p = 0.05$, the curve of g(MLat) obtained by spline function fitting is more smooth and can retain the original local fluctuations of N_e. Along the rising direction of MLat on the fitted curve, the gradient of N_e (∇N_e) is defined as the increment (or decrement) of spline lines N_e over increment of MLat degree. ∇N_e of the two events is shown in Fig. 1c. According to International Reference Ionosphere (IRI) model and summarized from massive observation data of DEMETER (Su et al. 2015), N_e decreases with the increase of MLat so that ∇N_e keeps a minus sign. However, the variations of N_e in Fig. 1b are different from the trend.

Geomagnetic activity

The SYM-H index is an index to measure the symmetrical disturbance of the horizontal geomagnetic field component (Wanliss and Showalter 2006). Compared with Dst, SYM-H has a high temporal resolution of 1 min and can describe the effects of the solar wind dynamic pressure variation. Here, we use the SYM-H index to analyze the geomagnetic activity when PLHR occurred in middle- and low-latitude zones. Figure 1d shows the fluctuation of the SYM-H index three days before events A and B. Its maximum value $\mathrm{SYM\text{-}H}_{3\mathrm{d\_max}}$ is only 19 nT, which means that both events occurred in the geomagnetically quiet period. To be clear, $\mathrm{SYM\text{-}H}_{3\mathrm{d\_max}}$ indices used below are the maximum value of 24 × 3 h before the moment when PLHR occurred.

Conjugate observation of PLHR

We have manually checked the orbits crossing both zones *N* and *S*. 22 events in daytime and 5 events in nighttime at *N* and 10 events in daytime at *S* are detected. Detailed orbits data are shown in Table 2. The geographical distribution of all PLHR events is shown in Fig. 2a, and many events occurred at revisit orbits every 13 days.

Due to the lower power consumption at night, for instance, the power consumption during daytime is about 1.5 times higher than during nighttime in China, the power of power line radiation decreases and may not reach the location of DEMETER. Moreover, the disappearance of the ionospheric D-layer at night will reduce the wave absorption, allowing lightning whistles, plasma hiss, and other natural and artificial waves in the same frequency band as PLHR penetrate the lower ionosphere

Table 1 Data of two typical PLHR events

Event	Date	Δf [Hz]	PSD [$\mu V^2 m^{-2}$ Hz^{-1}]	Total PSD [$\mu V^2 m^{-2}$]	SNR [dB]	MLat	*L*	PLE [$\mu V^2 m^{-2}$ Hz^{-1}]
A	02/01/2010	+3	0.017	0.052	9.42	16.8–22°N	1.14–1.24	1.15
B	02/02/2010	0	0.022	0.048	11.38	22–33°S	1.20–1.75	No

Δf is the maximum frequency deviation of spectral lines from the exact harmonic frequencies of 50 Hz; PSD is the maximum peak power spectral density; Total PSD is the total power spectral density of PLHR spectral lines; SNR is the signal-to-noise ratio; MLat is the geomagnetic latitude; *L* is *L*-shell value; and PLE represents the peak power spectral density of PLE which accompanies PLHR

Table 2 The number of orbits at *N* and *S*

Zone	Months	Daytime orbits (Number of PLE)			Nighttime orbits (Number of PLE)		
		Total	With PLHR	Without PLHR	Total	With PLHR	Without PLHR
N	Apr–Sep	395 (149)	1 (1)	394 (148)	399 (36)	0 (0)	399 (36)
	Jan–Mar and Oct–Dec	426 (257)	21 (21)	405 (236)	455 (117)	5 (4)	450 (113)
S	Apr–Sep	56 (2)	0 (0)	56 (2)	53 (7)	0 (0)	53 (7)
	Jan–Mar and Oct–Dec	58 (6)	10 (0)	48 (6)	60 (1)	0 (0)	60 (1)

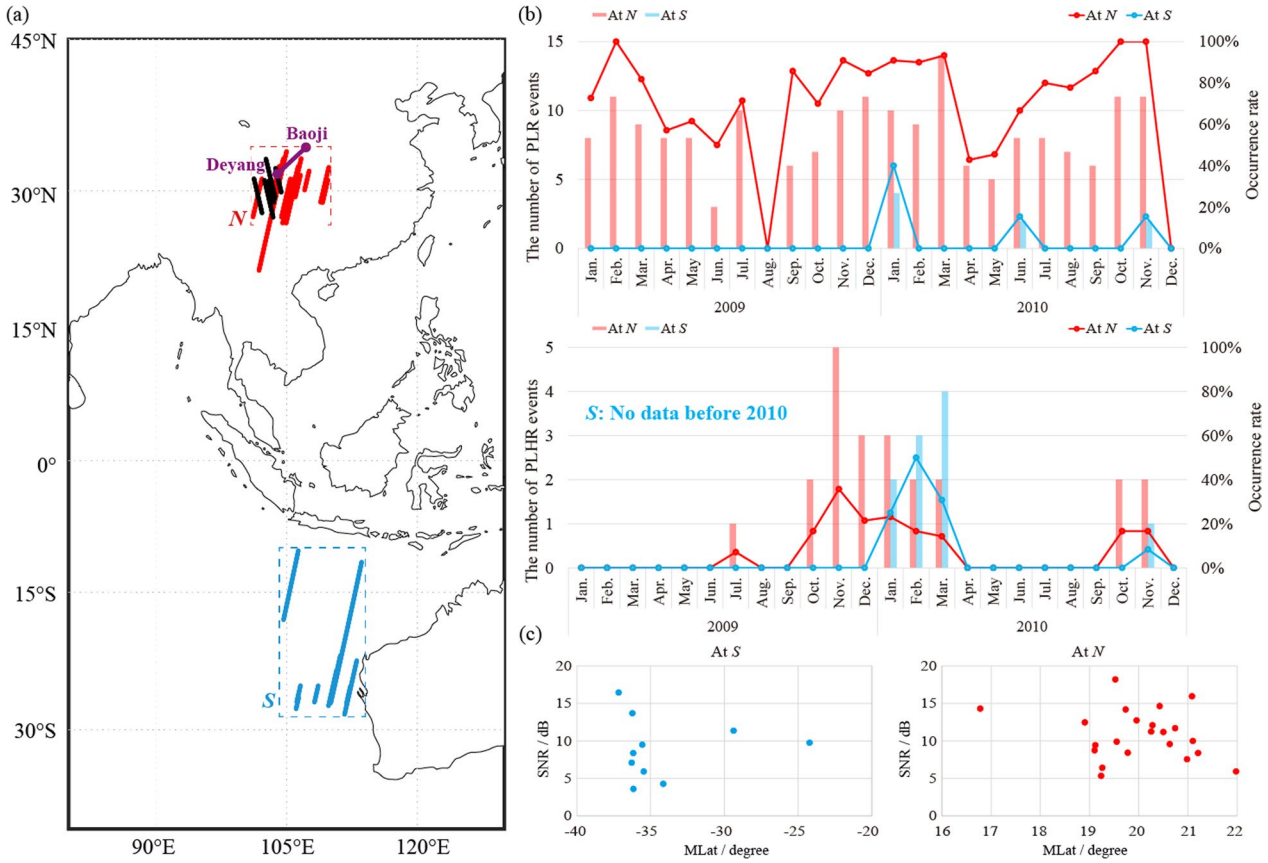

Fig. 2 PLHR events at conjugate zones. **a** Geographical projects of all PLHR events on the Earth's surface. The daytime events at zones *N* and *S* are shown in red and blue, respectively. All nighttime events are shown in black. **b** Monthly distribution of PLE and PLHR events. Bars in light red and blue show the number of PLHR orbits at *N* and *S*, respectively, and the lines show their occurrence rate every month. **c** SNR of all PLHR events. The horizontal axis represents the central MLat of each event

so that the background noise at the location of DEMETER is enhanced and PLHR is more difficult to be identified. The above factors lead to the number of PLHR events during nighttime is much smaller than during daytime (Němec et al. 2008; Wu et al. 2017). Here only the daytime PLHR events are statistically analyzed.

Statistical results

The monthly distribution of the number of PLHR events and the monthly occurrence rate, defined as the ratio of the number of events to the total number of orbits in a month, are shown in Fig. 2b. At *S* there are few PLE events, and their monthly occurrence rate is no more than 50%, but at *N* the monthly occurrence rate remains at a high level and even reaches 100% in February 2009 and in October and November 2010. Moreover, at *N* there were no PLHR events detected before June 2009, but approximately 45% of events were detected in winter of 2009 and 50% of events were detected in spring and winter of 2010. The abrupt increase in the second half of 2009 is easily connected with the great change in the ground power grid near the north footprint of *N* that ±500 kV Deyang-Baoji DC power project shown in Fig. 2a was put into operation. At *S* all PLHR events were detected in January, February, March, and November, 2010, synchronized with those at *N*. In general, PLHR is closely related to the ground power grid and is more likely to occur in spring and winter. This result is similar to that reported in Němec et al. (2015) and Wu et al. (2017), which should be attributed to the ionospheric condition and large variation of atmospheric noise at middle latitudes.

Statistics on the spectrums are shown in Table 3. At *N*, in addition to one event containing the harmonic spectral lines in the band of (1100–1700) Hz, all others contain only the spectral lines at approximately 4150/4250/4350/4450 Hz with $\triangle f \in (-4, 3)$ Hz. At *S*, all events contain only the spectral lines at approximately 4150/4250/4350/4450 Hz with $\triangle f \in (-8, 0)$ Hz. There was no correlation between the intensity of PLHR and the MLat (Fig. 2c). The average power spectral density is $(\overline{PSD}) = 0.033\ \mu V^2 m^{-2}\ Hz^{-1}$ with a standard

Table 3 Statistical values of all daytime events at *N* and *S*

Zone	MLat	*L*	Number	Δ*f* [Hz]	$\overline{\text{PSD}}$[μV²m⁻² Hz⁻¹]	$\overline{\text{SNR}}$[dB]
N	11°N–24°N	1.07–1.30	22	(−4, +3)	0.033	10.83
S	20°S–40°S	1.18–1.82	10	(−8, 0)	0.025	9.01

deviation 0.0246 and the average signal-to-noise is ($\overline{\text{SNR}}$)=10.83 dB with the standard deviation 3.26 at *N*. At S, ($\overline{\text{PSD}}$)=0.025 $\mu V^2 m^{-2}$ Hz^{-1} with the standard deviation 0.0249 and ($\overline{\text{SNR}}$)=9.01 dB with the standard deviation 3.86. It is worth mentioning that the power spectral densities of events at *N* are not always stronger than those at *S*, such as the events shown in Fig. 1.

The correlation between PLHR events and geomagnetic activities from July 2009 to December 2010 when PLHR events were detected is explored. The geomagnetic activity level is defined as follows (Loewe and Prlss 1997): quiet for SYM-H > − 30 nT, weak for − 30 nT > SYM-H > − 50 nT, and moderate for − 50 nT > SYM-H > − 100 nT. Comparison of SYM-H indices at both zones is shown in Fig. 3. At each zone, two tags are used for comparison. 'PLHR' and 'NORMAL' represent orbits with and without PLHR; 'exact' represents the time when PLHR was detected and 'pre3days' represents the previous 3 days of PLHR (taking the maximum value of SYM-H). At *N* the ratios of quiet activity along PLHR orbits during 'exact' and 'pre3days' are 100% and 90.9% which are larger than 95.5% and 76.0% along NORMAL orbits. At *S* the ratio of quiet activity along PLHR orbits is 90%, a little lower than 93.3% along NORMAL orbits during 'exact' time; the ratio of quiet activity along PLHR orbits is 80%, larger than 68.3% along NORMAL orbits during 'pre3days' time. It seems that PLHR tends to occur during geomagnetic quiet times, and the potential energetic electrons occurred after disturbed geomagnetic activity declared in Park and Helliwell (1978) do not beneficial for the occurrence of PLHR.

The numbers of orbits in different cases are shown in Table 4. Němec et al. (2006) mentioned that the peak intensity of PLHR increases when the geomagnetic activity (Kp index) becomes strong. However, according to the statistics on the PSD and the SYM-H index of our detected events shown in Fig. 4, nothing special correlation can be seen.

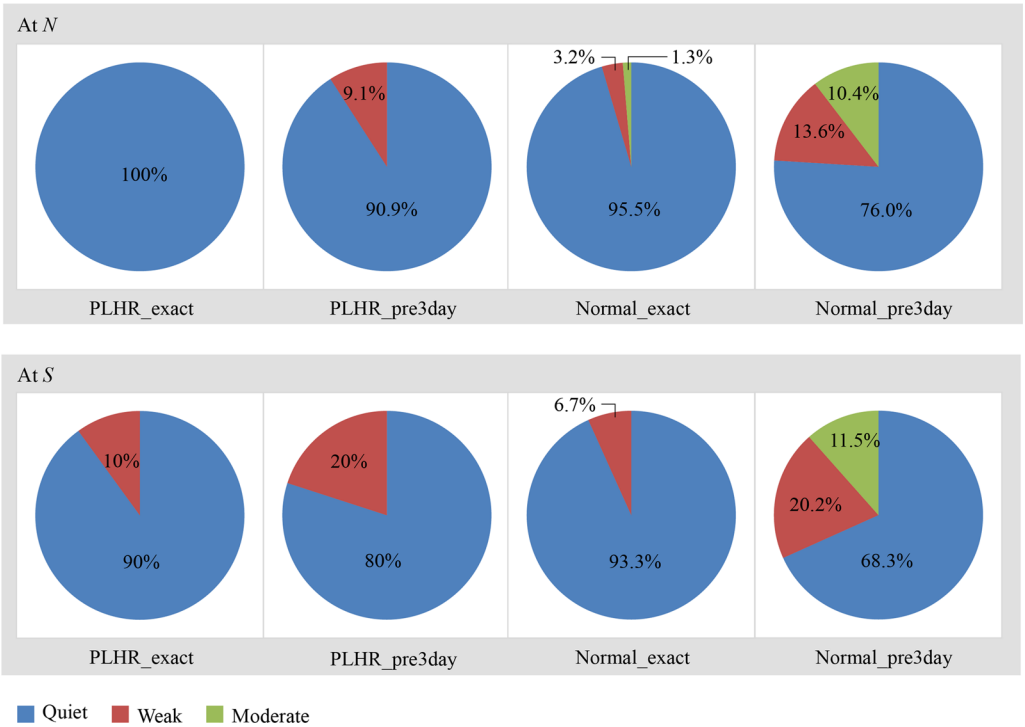

Fig. 3 Distribution of SYM-H

Table 4 Detailed orbit data at *N* and *S* during daytime

Zone	Months	'Exact' (number of quiet)		'pre3days' (number of quiet)	
		'PLHR'	'Normal'	'PLHR'	'Normal'
N	Apr–Sep	1 (1)	83 (77)	1 (1)	83 (53)
	Jan–Mar and Oct–Dec	21 (19)	71 (70)	21 (19)	71 (64)
S	Apr–Sep	0 (0)	56 (50)	0 (0)	56 (29)
	Jan–Mar and Oct–Dec	10 (9)	48 (47)	10 (8)	48 (42)

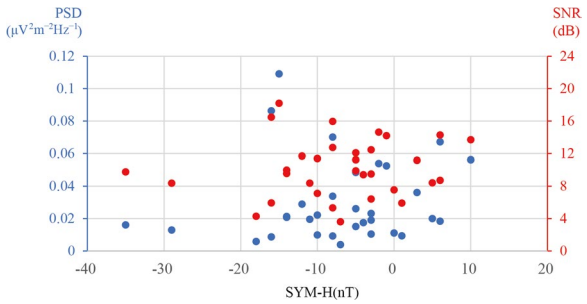

Fig. 4 Correlation between PSD and SNR of PLHR and SYM-H. PSD on the left and SNR on the right of *y*-axis

Statistics of N_e

The fluctuations of N_e and ∇N_e along all PLHR orbits are shown in Fig. 5. More than 77% of daytime events at *N* with $\overline{\mathrm{PSD}} = 0.0316\ \mu\mathrm{V}^2\mathrm{m}^{-2}\ \mathrm{Hz}^{-1}$ ($\overline{\mathrm{SNR}} = 10.82$ dB) and 80% at *S* with $\overline{\mathrm{PSD}} = 0.0291\ \mu\mathrm{V}^2\mathrm{m}^{-2}\ \mathrm{Hz}^{-1}$ ($\overline{\mathrm{SNR}} = 9.99$ dB) occurred near local troughs or crests of N_e where sign of ∇N_e changes, similar to the typical events described in Fig. 1.

Since most PLHR events occurred during the geomagnetic quiet period, numbers of the PLHR and NORMAL orbits during the quiet period shown in Table 4 are chosen to analyze the dependence of PLHR on ∇N_e. Figure 6 shows the variation of ∇N_e during daytime at the Northern and Southern Hemispheres from October to December and from January to March. ∇N_e along all orbits within per 1° MLat is shown by dots, and 15–85 quantiles of the values of ∇N_e per 1° MLat are shown by bars. PLHR orbits are shown in red, NORMAL orbits are shown in green, and ∇N_e obtained from IRI model is shown in black. The IRI model is a general mathematical model based on a lot of observed data, while the data of DEMETER reflect the real state of the ionosphere at a given moment (Ignoring the impact of the payloads' accuracy). By comparing the results from the IRI model and DEMETER, the difference between the actual and general state of the ionosphere can be more clearly illustrated during the occurrence of PLHR. According to IRI, ∇N_e keeps negative because N_e decreases with the increase of latitude, and the positive values in 5°N–8°N MLat are resulted from equatorial ionization anomaly. According to the data of DEMETER, ∇N_e maintains negative values along the daytime orbits without PLHR at 5°N–14°N MLat. However, when PLHR occurs at 11°N–24°N MLat, ∇N_e abruptly changes from negative values to positive values. At *S*, there are only 10 PLHR orbits and the variation of ∇N_e is not obvious, which is similar as that along the orbits without PLHR.

Results and discussion

The number of PLHR events at *N* suddenly increased in the second half of 2009 which is the commissioning time of the ultrahigh power project. All events have spectral lines at frequencies approximately 4150/4250/4350/4450 Hz and are accompanied by PLE. These facts effectively illustrate that the ultrahigh power project at *N* is a steady power harmonic source and events at *N* are originated from it. While at *S*, the number of PLHR events increased in 2010 and we have no way to determine whether PLHR existed before 2010 for lack of burst-mode data. PLHR events at *S* are all at approximately 4150/4250/4350/4450 Hz and in the same month of those at *N*. Besides that, no PLE was detected along PLHR orbits at *S*. We deduce that PLHR at *S* resulted from the propagation of PLHR at *N*.

According to Helliwell et al. (1975), VLF radiations can be observed simultaneously at conjugate regions, during which process amplification occurred in the equatorial plane through a feedback process based on electron cyclotron resonance. Using the ray-tracing methodology (Bortnik 2004), our calculations show 4 kHz-PLHR at 30° geomagnetic latitude with a vertical initial wave normal angle prefers to migrate to a higher *L*-shell and finally settle on a particular *L*-shell about 1.6 which is above the DEMETER orbit. PLHR at *S* with higher intensity at higher *L*-shell should result from one hop of PLHR at *N* crossing the equator. If there were another satellite at higher altitude, more events could be observed since PLHR settled there.

It is notable that, from ground-based observations, Park and Helliwell (1978) indicated that PLHR tends to occur during quiet times immediately following disturbances (preceding 24 h), when good propagation conditions are combined with the enhanced electron fluxes needed for strong wave–particle interactions. However, our events were mainly detected during geomagnetic quiet time and disturbed geomagnetic activities did not show preference three days before PLHR. And no correlation has been found between the intensity of PLHR and SYM-H index. The above results are in contradiction with those declared in Park and Helliwell (1978) and Němec et al. (2006). Geomagnetic disturbances seem to

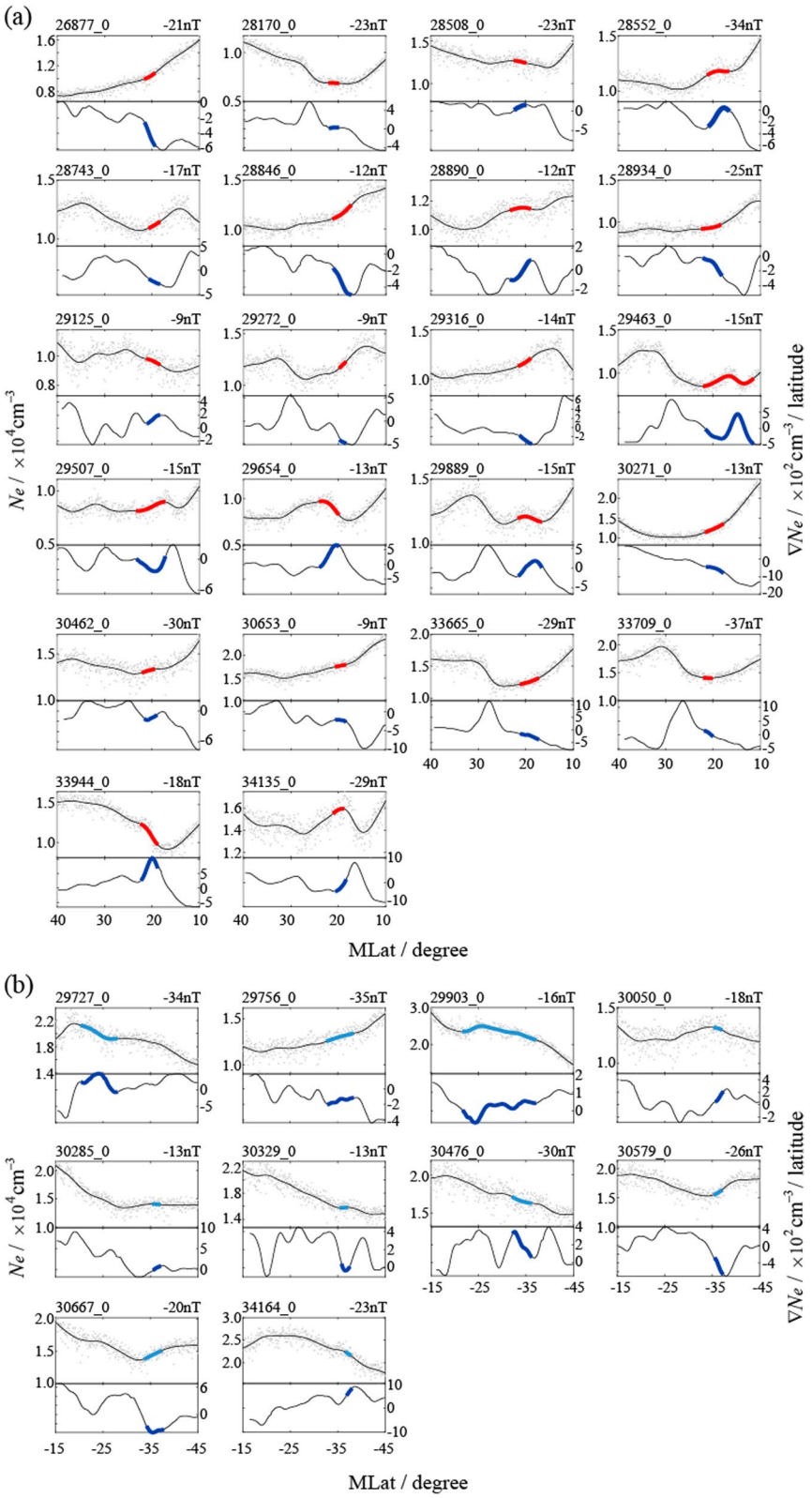

Fig. 5 Fluctuation of N_e along all identified PLHR orbits. Orbits at *N* and at *S* share the same horizontal coordinate. **a** At *N*. **b** At *S*. Texts on every panel show orbit number (left) and SYM-H_{3d_max} (right)

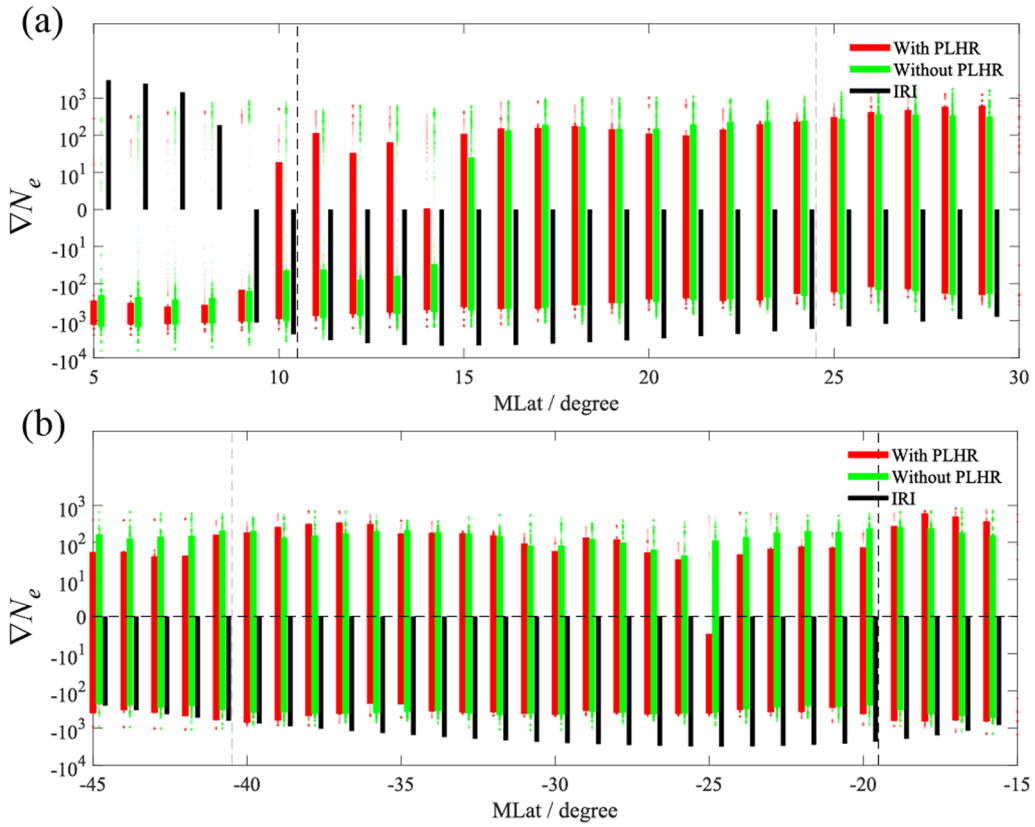

Fig. 6 Variation of ∇N_e. ∇N_e along the orbits with and without PLHR in Jan–Mar and Oct–Dec compared with IRI model at *N* (**a**) and at *S* (**b**). Orbits with PLHR are shown in red, orbits without PLHR are shown in green and ∇N_e obtained from IRI model is shown in black. ∇N_e along all orbits within per 1° MLat is shown by dots, and 15–85 quantiles of the values of ∇N_e per 1° MLat are shown by bars

have no effect on the occurrence, propagation and amplification of PLHR.

As shown in Fig. 6a, when PLHR occurs in the range of 11°N–24°N MLat during the daytime, ∇N_e has obvious change, indicating that PLHR depends on not only the strong radiation from the power grid but also the variation of plasma density. According to propagation mechanism of whistler mode wave given by Walker (1976), the abrupt variation of N_e creates a favored condition for PLHR wave propagating between hemispheres. Due to the constraints of satellite-based observations, it is currently difficult to confirm the interdependence between PLHR and plasma density, but this is a potential direction to continue to explore the mechanism of PLHR in the future.

The frequency drift of parallel PLHR spectral lines with time at each hemisphere and the frequency deviation from the exact power harmonic frequencies have also attracted our attention. Within PLHR duration (no more than 10 min), 55% events have the frequency drift less than 1 Hz which are hard to be identified, and 18% events have the drift in range of 1–5 Hz like a V shape, similar to that discussed by Němec et al. (2021), and can be explained by the Doppler shift. The remainder may be due to whistler mode instability during a gyro-resonance interaction between PLHR waves and particles in an inhomogeneous medium (Parrot 1994). For those events with the frequency drifts less than 1 Hz, their frequency deviations from the exact harmonic frequencies of 50 Hz are in $(-4, +3)$ Hz at *N* and in $(-8, 0)$ Hz at *S*. The frequency deviation at *N* may be attributed to the frequency fluctuation in the practical power grid. According to the national standard GB/T15945 of China, when the fundamental frequency fluctuation of reaches level A, its allowable deviation is in $(-0.05, +0.05)$ Hz, so the deviations of the 83rd, 85th, 87th, and 89th harmonics are within $(-4.45, +4.45)$ Hz. If PLHR waves at *S* are thought to result from the hop across the equator, then the deviation may be due to the nonlinear interaction of cyclotron resonant electrons with a narrow band whistler wave.

According to the theory presented by Helliwell (1967), Parrot (1994) and Sudan and Ott (1971), If wave-particle cyclotron resonance occurs at equatorial region, in order to maintain it, the wave frequency must be changed

Table 5 Frequency deviations of typical events

f / Hz	Along 298,890 at *N*		Along 306,670 at *S*	
	$\Delta f_{Observed}$	$\Delta f_{Calculated}$	$\Delta f_{Observed}$	$\Delta f_{Calculated}$
4150	(2, 4)	3.2	(−4, −2)	− 3.8
4250	(1, 4)	2.8	(−5, −2)	− 4.1
4350	(2, 4)	2.9	(−4, 0)	− 4.0
4450	(3, 4)	3.1	(−4, 0)	− 4.0

synchronously to match the change in the electron cyclotron frequency. Considering the changes in the equatorial geomagnetic field and electron density, the frequency deviation (Δf) can be calculated by the formula as

$$\Delta f = \frac{3\lambda}{1+2\lambda}\left[1+\frac{1-\lambda}{3}\tan^2\alpha\right]\Delta f_{ce} - \frac{2\lambda(1-\lambda)}{1+2\lambda}\frac{\Delta N_e}{N_e}f_{ce}, \quad (2)$$

where $\lambda = f/f_{ce}$, f is the wave frequency, f_{ce} is the electron cyclotron frequency, α is the pitch angle of electron, Δf_{ce} is the variation of electron cyclotron frequency, and ΔN_e is the variation of electron density. It is difficult to obtain the real values of magnetic flux density and electron density along a geomagnetic field line, here we use the local variations at equatorial region observed by DEMETER to approximate them. Taking events along orbits 298,890 at N and 306,670 at S as an example, through calculations the frequency deviations are shown in Table 5 which are in agreement with the observed values. The interaction between PLHR and energetic electrons still needs to be demonstrated in the future.

With the development of a large-scale ultrahigh voltage power grid, its significant value as a controllable and artificial large transmitter in understanding the ionospheric state and the magnetosphere–ionosphere coupling mechanism, as well as controlling the motion of energetic electrons in the magnetosphere, deserves serious attention.

Abbreviations

PLHR	Power line harmonic radiation
PLE	Power line emission
PSD	The peak power spectral density of PLHR spectral lines
SNR	Signal-to-noise ratio, the ratio of the maximum PSD to the average background noise wave density
IRI	International Reference Ionosphere
DEMETER	Detection of Electro-Magnetic Emissions Transmitted from Earthquake Regions
SYM-H	Symmetric portion of the horizontal component magnetic field

Acknowledgements

The authors thank Michel Parrot (LPC2E/CNRS Orléans, Orléans, France) for useful discussions and suggestions.

Author contributions

JW and CY conceived and supervised the project. JW, ZW, and JZ designed the method and performed the formal analysis. JW, JZ, ZW, and CY wrote the original draft, and LX revised the manuscript. All the authors read and approved the final manuscript.

Funding

This work was supported by National Natural Science Foundation of China (51777006, 41974191) and Beijing Natural Science Foundation (8222063).

Availability of data and materials

Data of DEMETER satellite can be obtained at https://cdpp-archive.cnes.fr/ in the "DEMETER Mission" dataset in the navigation pane after asking for a permanent account from CNES. SYM-H index is provided by World Data Center (http://wdc.kugi.kyoto-u.ac.jp/wdc/Sec3.html).

Declarations

Ethics approval and consent to participate

Not applicable.

Consent for publication

Not applicable.

Competing interests

The authors declare that they have no competing interests.

Author details

[1]School of Automation Science and Electrical Engineering, Beihang University, Beijing, China. [2]Institute of Space Physics and Applied Technology, Peking University, Beijing, China. [3]China Electric Power Research Institute, Beijing, China.

Received: 21 December 2022 Accepted: 10 April 2023
Published online: 04 May 2023

References

Bell TF, Luette JP, Inan US (1982) ISEE 1 observations of VLF line radiation in the Earth's magnetosphere. J Geophys Res 87(A5):3530–3536. https://doi.org/10.1029/JA087iA05p03530

Bortnik J (2004) Precipitation of radiation belt electrons by lightning-generated magnetospherically reflecting whistler waves. Dissertation, Stanford University

Dudkin F, Korepanov V, Dudkin D, Pilipenko V, Pronenko V, Klimov S (2015) Electric field of the power terrestrial sources observed by microsatellite Chibis-M in the Earth's ionosphere in frequency range 1–60 Hz. Geophys Res Lett 42(14):5686–5693. https://doi.org/10.1002/2015GL064595

Guo Q, Wu J, Yue C, Xie L (2019) Correlation between power line harmonic radiation and magnetospheric line radiation over China. IEEE Access 7:146857–146865. https://doi.org/10.1109/ACCESS.2019.2946099

Helliwell RA (1965) Whistlers and related ionospheric phenomena. Stanford University Press, Stanford

Helliwell RA (1967) A theory of discrete VLF emissions from the magnetosphere. J Geophys Res 72(19):4773–4790. https://doi.org/10.1029/JZ072i019p04773

Helliwell RA, Katsufrakis JP, Bell TF, Raghuram R (1975) VLF line radiation in the earth's magnetosphere and its association with power system radiation. J Geophys Res 80(31):4249–4258. https://doi.org/10.1029/JA080i031p04249

Lagoutte D et al (2006) The DEMETER science mission center. Planet Space Sci 54:428–440. https://doi.org/10.1016/j.pss.2005.10.014

Loewe CA, Prlss GW (1997) Classification and mean behavior of magnetic storms. J Geophys Res Space Physics 102(A7):14209–14213. https://doi.org/10.1029/96ja04020

Luette JP (1983) Power line radiation in the magnetosphere. Dissertation, Stanford University

Manninen J (2005) Some aspects of ELF-VLF emissions in geophysical research. Dissertation, University of Oulu

Němec F, Santolík O, Parrot M, Berthelier JJ (2006) Power line harmonic radiation (PLHR) observed by the DEMETER spacecraft. J Geophys Res 111:A04308. https://doi.org/10.1029/2005JA011480

Němec F, Santolík O, Parrot M, Berthelier JJ (2007a) Power line harmonic radiation: a systematic study using DEMETER spacecraft. Adv Space Res 40(3):398–403. https://doi.org/10.1016/j.asr.2007.01.074
Němec F, Santolík O, Parrot M, Berthelier JJ (2007b) Comparison of magnetospheric line radiation and power line harmonic radiation: a systematic survey using the DEMETER spacecraft. J Geophys Res 112:A04301. https://doi.org/10.1029/2006ja012134
Němec F, Santolík O, Parrot M, Bortnik J (2008) Power line harmonic radiation observed by satellite: properties and propagation through the ionosphere. J Geophys Res 113:A08317. https://doi.org/10.1029/2008ja013184
Němec F, Parrot M, Santolík O (2010) Influence of power line harmonic radiation on the VLF wave activity in the upper ionosphere: Is it capable to trigger new emissions? J Geophys Res 115:A11301. https://doi.org/10.1029/2010JA015718
Němec F, Parrot M, Santolík O (2015) Power line harmonic radiation observed by the DEMETER spacecraft at 50/60 Hz and low harmonics. J Geophys Res Space Physics 120(10):8954–8967. https://doi.org/10.1002/2015ja021682
Němec F, Santolík O, Parrot M (2021) Doppler shifted alpha transmitter signals in the conjugate hemisphere: DEMETER spacecraft observations and raytracing modeling. J Geophys Res Space Phys. https://doi.org/10.1029/2020JA029017
Nunn D, Manninen J, Turunen T, Trakhtengerts V, Erokhin N (1999) On the nonlinear triggering of VLF emissions by power line harmonic radiation. Ann Geophys 17(1):79–94. https://doi.org/10.1007/s00585-999-0079-4
Park CG, Chang DCD (1978) Transmitter simulation of power line harmonic radiation effects in the magnetosphere. Geophys Res Lett 5(10):861–864. https://doi.org/10.1029/GL005i010p00861
Park CG, Helliwell RA (1978) Magnetospheric effects of power line radiation. Science 200(4343):727–730. https://doi.org/10.1126/science.200.4343.727
Park CG, Helliwell RA (1981) Power line radiation in the magnetosphere. Adv Space Res 1(2):423–437. https://doi.org/10.1016/0273-1177(81)90317-3
Park CG, Helliwell RA, LeFeuvre F (1983) Ground observations of power line radiation coupled to the ionosphere and magnetosphere. Space Sci Review 35(2):131–137. https://doi.org/10.1007/BF00242240
Parrot M (1994) Observations of power line harmonic radiation by the low-altitude AUREOL 3 satellite. J Geophys Res 99(A3):3961–3969. https://doi.org/10.1029/93JA02544
Parrot M (2018) DEMETER observations of manmade waves that propagate in the ionosphere. C R Phys 19(1–2):26–35. https://doi.org/10.1016/j.crhy.2018.02.001
Parrot M, Němec F (2009) MLR events and associated triggered emissions observed by DEMETER. Adv Space Res 44(9):979–986. https://doi.org/10.1016/j.asr.2009.07.001
Parrot M, Němec F, Santolík O (2014) Statistical analysis of VLF radio emissions triggered by power line harmonic radiation and observed by the low-altitude satellite DEMETER. J Geophys Res 119(7):5744–5754. https://doi.org/10.1002/2014JA020139
Pilipenko VA, Fedorov EN, Mazur NG, Klimov SI (2021) Electromagnetic pollution of near-Earth space by power line emission. Solar-Terrestrial Phys 7(3):105–113. https://doi.org/10.12737/stp-73202107
Rodger CJ, Thomson NR, Dowden RL (1995) VLF line radiation observed by satellite. J Geophys Res 100:5681–5689. https://doi.org/10.1029/94ja02865
Su F, Wang W, Burns AG, Yue X, Zhu F (2015) The correlation between electron temperature and density in the topside ionosphere during 2006–2009. J Geophys Res Space Physics 120:10724–10739. https://doi.org/10.1002/2015JA021303
Sudan RN, Ott E (1971) Theory of triggered VLF emissions. J Geophys Res 76(19):4463–4476. https://doi.org/10.1029/JA076i019p04463
Thorne RM, Tsurutani BT (1979) Power line harmonic radiation: can it significantly affect the Earth's radiation belts? Science 204:839–841. https://doi.org/10.1126/science.204.4395.839
Thorne RM, Tsurutani BT (1981) Comment on 'Sunday decreases in magnetospheric wave activity' by C. G. Park and T. R. Miller. J Geophys Res 86:1639–1641. https://doi.org/10.1029/JA086iA03p01639
Tomizawa I, Yoshino T (1985) Power line radiation observed by the satellite "OHZORA." J Geomagn Geoelectr 37(3):309–327. https://doi.org/10.5636/jgg.37.309
Walker ADM (1976) The theory of whistler propagation. Rev Geophys Space Phys 14(4):629–638. https://doi.org/10.1029/RG014i004p00629
Wanliss JA, Showalter KM (2006) High-resolution global storm index: Dst versus SYM-H. J Geophys Res 111(A2):A0220. https://doi.org/10.1029/2005JA011034
Wu J, Zhang C, Zeng L, Ma QS (2017) Systematic investigation of power line harmonic radiation in near-Earth space above China based on observed satellite data. J Geophys Res 122:3448–3458. https://doi.org/10.1002/2016JA023131
Wu J, Zhang J, Xie L (2022) Uncommon electromagnetic radiations related to extra-high voltage/ultra-high voltage power projects in China. Front Environ Sci. https://doi.org/10.3389/fenvs.2022.902508

Publisher's Note